

Measurement of weak branching out of the (near-) two-level system $\text{Ba } 6s6p \ ^1P_1 \leftrightarrow 6s^2 \ ^1S_0$

G. K. Gerke and B. A. Bushaw

Pacific Northwest Laboratory, Richland, Washington 99352

(Received 16 March 1987; revised manuscript received 28 September 1987)

Weak branching out of the $6s^2 \ ^1S_0 \leftrightarrow 6s6p \ ^1P_1$ two-level system to the metastable $6s5d \ ^{1,3}D$ states has been measured for ^{138}Ba using cw-resonance ionization mass spectrometry on an optically pumped atomic beam. A branching ratio (inverse branching fraction) of 440 ± 40 was obtained.

INTRODUCTION

Two-level atomic systems are important in fundamental photophysical studies such as the slowing and trapping of atoms¹ and the preparation of magnetically aligned and oriented atomic beams.² They are also important in ultratrace analysis with photon-burst detection,³ isotope separation,⁴ and isotope enrichment by photodeflection.⁵ The degree of success in these experiments depends upon the number of times that an atom can be cycled through the two-level system by optical excitation. Alkaline-earth metals form relatively good two-level systems between the 1S_0 ground state and the first 1P_1 state, but are limited (except in Be and Mg) by branching to intermediate 1D_2 and 3D_2 metastable states. Despite the importance of these weak transitions, existing measurements of their strengths in barium are in substantial disagreement and values for the branching ratio range from 24 to ≥ 700 .⁶⁻¹⁷ Only two of these values^{11,13} were determined by direct measurement while the others were deduced from indirect measurements or theoretical calculations. Niggli and Huber¹⁴ have recently made a critical evaluation of these reported values and selected as most probable a value of 290 ± 40 .

Figure 1 shows the pertinent energy levels in barium and the excitation scheme we used for measuring the branching to the $^{1,3}D$ metastable states. Illumination of an atomic beam of barium with 553.7-nm radiation over a well-defined interaction region causes repeated excitation of the $6s^2 \ ^1S_0 \leftrightarrow 6s6p \ ^1P_1$ transition. For a small fraction of the excitations the 1P_1 excited state decays to the $^{1,3}D$ states rather than the ground state, and these atoms are not available for further cycling. We measure the population remaining in the $^1S_0 \leftrightarrow ^1P_1$ two-level system by photoionization of the 1P_1 state downstream of the pump region.

Two complementary pump-probe experiments have been used to investigate the branching ratio. In one set of experiments the dye-laser frequency is locked at the center of the $^1S_0 \leftrightarrow ^1P_1$ resonance and the degree of pumping is measured as a function of the pump path length. As the path length is increased, population trapped in the D states increases, and a decay in the two-level system population is observed. The decay is nearly exponential but shows slight curvature due to varying interaction times of the velocity distribution and to recoil

Doppler shifting.¹⁸ Recoil shifting is due to changes in an atom's velocity from repeated absorption of photons. Each photon's absorption or emission carries h/λ momentum with it. While all momentum gained from absorption (from the laser) is in one direction, spontaneous emission is symmetric and its momentum transfer averages to zero over a number of excitation cycles. The net effect is to push atoms in the direction of laser propagation. The resulting Doppler shift may either push the atom into resonance if the laser is tuned to the high-energy side of the rest frequency, or push it (further) out of resonance when the laser frequency is less than or equal to the rest frequency.

In the second type of experiment the pump path length is held constant while the dye-laser frequency is scanned across the $^1S_0 \leftrightarrow ^1P_1$ resonance. This yields spectra with distorted line shapes due to optical pumping. Since pumping to the D states is strongest on line center, this can result in dips or inversions in the spectra, particularly when there is some saturation in the probe region. For simplicity we refer to the two types of experiments as "decay" and "inversion" measurements. Both experiments were run at a variety of pump-and-probe laser in-

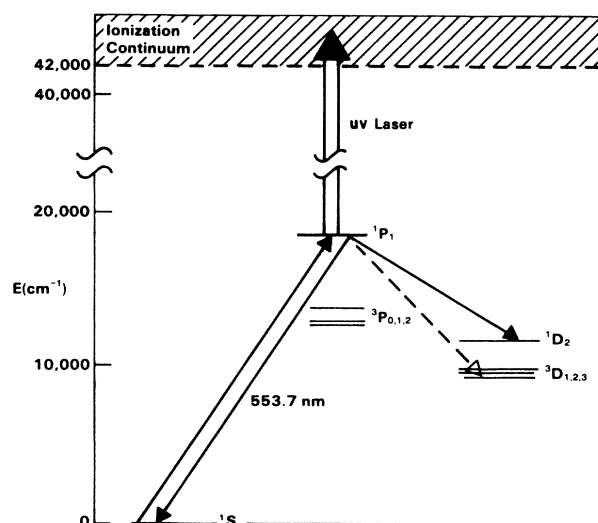


FIG. 1. Energy-level diagram for the low-lying states in barium used in determining the branching ratio $A(^1P_1 \leftrightarrow ^1S_0) / \sum A(^1P_1 \leftrightarrow D)$ for barium.

tensities and spectra were fit to a modelling equation which includes residual Doppler broadening due to beam divergence, the axial velocity distribution of the atomic beam, pump-and-probe laser intensities and spatial distributions, and recoil shifts.

EXPERIMENTAL

Figure 2 shows the experimental arrangement used for the measurements. The collimated (15 mrad full angle) atomic beam of barium (natural abundances) is generated by heating solid barium metal with an oven to typically 500°C. This results in a beam density of 10^5 – 10^6 atoms/cm³ in the interaction regions. A fringe-offset locking technique which has been described previously¹⁹ stabilizes a single-frequency dye laser (Coherent 599-21) by referencing to a single-frequency He-Ne laser (Laboratory for Science model 200). This computer-controlled feedback system allows either scanning or holding at a fixed frequency with drift stability of 0.5 MHz/h. Most of the dye-laser output is spatially filtered and expanded ($\sim 50\times$). The central portion is masked and compressed along the atomic beam axis by a cylindrical telescope into a spatially uniform (to within $\pm 10\%$) 1.0×0.3 -cm² rectangular pump beam. A motor-driven knife edge is translated across the beam to control the actual illumination path length. Laser powers were measured with two NBS traceable power meters (agreement within 5%) and intensity distributions were determined by translating a pinhole or slit across the beams with photodiode detection. During the experiments, the integrated pump beam intensity was monitored with a monochromator and photomultiplier after leaving the vacuum chamber.

Part of the same dye-laser output is used to form the probe beam, which enters the crossed-beam ionizer head of a quadrupole mass spectrometer and perpendicularly intersects the atomic beam. The probe beam overlaps the

focused ultraviolet output (75 μ m full width at half maximum, 2 W typical) of an argon-ion laser (Coherent I-100) which ionizes atoms in the 1P_1 state, but which has insufficient photon energy to ionize atoms trapped in the D states. Special care is taken to minimize optical pumping in the probe region by using a knife edge to trim the probe beam such that its upstream edge coincides with the uv beam.

Parallel alignment of the pump and probe beams is critical. Misalignment introduces a Doppler effect that can shift the position of the dip observed in line inversion spectra, as has been observed previously in experiments on hyperfine optical pumping.²⁰ To avoid this complication, the two beams were aligned to within 1 mrad, corresponding to a relative Doppler shift of less than 1 MHz.

MODEL CALCULATIONS

Modelling of the observed ion-detection rate R for the decay and inversion measurements allows for changes in the experimental variables of laser frequency and pump path length according to

$$R(v, l) = \int_{-r}^r \int_0^\infty N(x)N(v) \times \sum_{n=0}^{\infty} [P(n, a(v, x))L(n)\xi(n, v, x)] dv dx. \quad (1)$$

The component terms, which will be discussed below, include $N(x)dx$ and $N(v)dv$ which are, respectively, the spatial and axial velocity distributions for the atomic beam, $P(n, a(v, x))$ which is the distribution of the number of excitations for a particular space-velocity group, $L(n)$ which describes the losses to the metastable states, and $\xi(n, v, x)$ which is the probe beam detector function. The average number of excitations $a(v, x)$ and the probe detector function $\xi(n, v, x)$ are implicitly functions of the

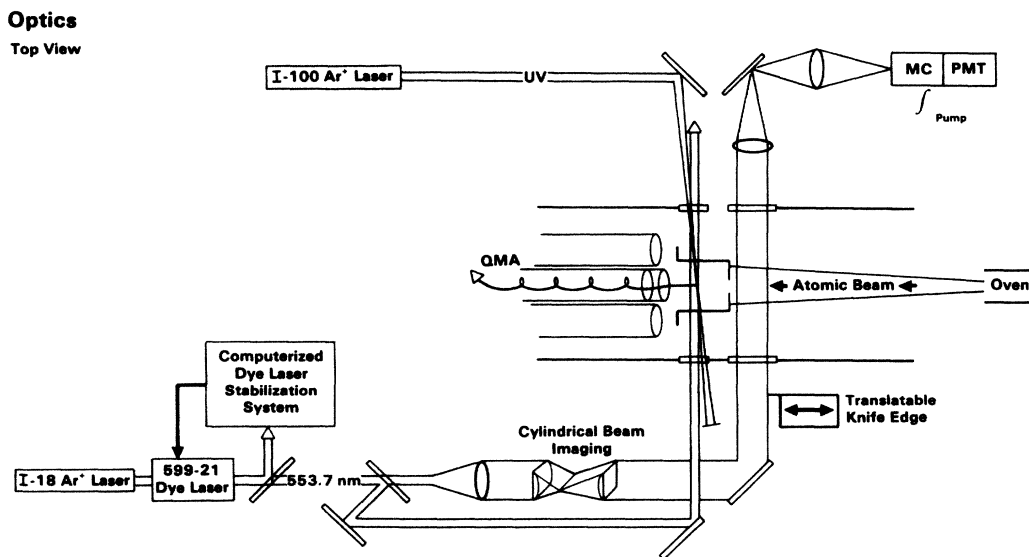


FIG. 2. Experimental arrangement. Abbreviations are MC: monochromator; PMT: photomultiplier tube; QMA: quadrupole mass analyzer.

laser frequency, intensity and path length. Holding laser frequency ν constant and evaluating Eq. (1) for different interaction path lengths l corresponds to the fixed frequency decay experiments and holding l constant and evaluating for different ν corresponds to the line inversion experiments.

$N(x)dx$ is the spatial distribution of atoms along the axis of laser propagation and is due to the divergence of the atomic beam and finite beam apertures. This distribution (with $x=0$ at the center of the atomic beam) will determine the initial Doppler shift of an atom, $\delta_0 = \nu_0(xv/dc)$, where ν_0 is the rest frequency of the transition, x is the transverse position of the atom, v is the atomic velocity, d is the distance from the atomic beam source, and c is the speed of light. With our particular geometry, $N(x)dx$ is constant over $-r$ to r , where r is the radius of the final atomic beam aperture.

The distribution of atomic velocities for a collimated atomic beam is given by²¹

$$N(v)dv = 2\alpha^{-4}v^3 \exp(-v^2/\alpha^2)dv, \quad (2)$$

where $\alpha = (2kT/m)^{1/2}$, k is Boltzmann's constant, T is the temperature in K, and m is the atomic mass.

$P(n, a(v, x))$ is the probability that an atom will experience exactly n excitations if an ensemble of atoms (of the same v and x) experiences an average of a excitations. For resonance excitation of a two-level atom this distribution may deviate slightly from Poissonian,²² however, for the experiments described here, where the number of excitation cycles is large, the distribution about the average a is narrow and the average could be used instead of the distribution. Using the average rather than integrating over the distribution enhanced computational speed yet introduced errors of less than 0.5%. Calculation of the number of excitations is complicated by the recoil shift which causes the excitation rate to vary continuously as the atom traverses the pump region. However, with constant pump laser intensity, the recoil velocity may be found in closed form by solving the cubic equation⁵ for the final transverse velocity v_f ,

$$v_f^3 - v_0^3 + 3\lambda\delta(v_f^2 - v_0^2) + 3\lambda^2(\Delta^2 + \delta^2)(v_f - v_0) - (3\Delta^2\lambda hz/m\tau v_z)f_0 = 0, \quad (3)$$

where v_0 is the initial transverse velocity, λ the wavelength of the transition, δ the laser detuning from the rest frequency, Δ the power broadened linewidth [half width at half maximum (HWHM)] given by $\Delta = \Gamma(1 + 2I/I_s)^{1/2}$, where Γ is the natural linewidth, τ the lifetime of the upper state, z the illuminated path length, and v_z the velocity along the atomic beam axis. The fraction of time an atom spends in the upper state on line center is given by $f_0 = (2 + I_s/I)^{-1}$, where I is the laser intensity and I_s the saturation intensity, which we define as the point where the rates of spontaneous and stimulated emission are equal. For the studied transition $I_s = 29.3$ mW/cm². The number of excitations is the total momentum imparted $m(v_f - v_0)$ divided by the momentum imparted per photon absorption (h/λ),

$$n = (m\lambda/h)(v_f - v_0). \quad (4)$$

The losses to the D states depend upon the actual number of excitation cycles which the atom experiences and is given by

$$L(n) = \exp\left[-n \sum A(^1P_1 \leftrightarrow D) / A(^1P_1 \leftrightarrow ^1S_0)\right], \quad (5)$$

where $A(^1P_1 \leftrightarrow ^1S_0) / \sum A(^1P_1 \leftrightarrow D)$, the Einstein spontaneous emission coefficient for the two-level transition divided by the sum of all coefficients for transitions which result in trapping, is defined as the branching ratio. The final term in Eq. (1) is the probe beam detection function which describes the probability for ionizing atoms which enter the probe region in the ground state,

$$\xi(n, v, x) = \epsilon[1 - \exp(-\sigma Ift)], \quad (6)$$

where ϵ represents the detector and transmission efficiency of the mass spectrometer, σ is the cross section for photoionization from the 1P_1 state by the ultraviolet laser with intensity I , f is the fraction of time spent in the 1P_1 state, and t is the time the atom takes to traverse the ionization region. The fraction of time spent in the upper state, f , depends upon the intensity and frequency of the probe dye laser as well as the initial and pump-induced Doppler shifts,

$$f = (2 + I_s/I_d)^{-1} \left[1 + \left[\frac{\nu_0 - (\nu + \delta_0 + \delta_n)}{\Delta_d} \right]^2 \right]^{-1}, \quad (7)$$

where the first term is the fraction of time the atom would spend in the 1P_1 state without any frequency shifts, and the second term gives the reduction in this fraction due to laser detuning, initial Doppler shift δ_0 , and recoil shift δ_n . The power-broadened linewidth (HWHM) for the probe laser is Δ_d .

Because of the relatively low intensity of the ultraviolet laser ($\sim 4 \times 10^4$ W/cm²) and the short transverse path length, the probability for ionization is low. Thus, in Eq. (6) the product $\sigma Ift \ll 1$ and the first expansion term, $\xi = \epsilon\sigma Ift$, is a valid approximation. A value of $\sigma Ift \sim 10^{-2}$ at the mean velocity is consistent with a cross section of $\sigma = 10^{-18}$ cm² and experimentally measured detection efficiencies. The linearity is also experimentally verified by the lack of saturation effects when the intensity of the ionization laser is varied.

RESULTS AND DISCUSSION

Initial experiments were conducted with comparable pump and probe laser intensities. With laser intensities close to saturation and a fixed pump path length l , the dye laser was scanned over the resonant frequency resulting in line inversion profiles. Figure 3 shows two sets of experimental spectra with different pump and probe parameters and these are compared to curves generated by numerical integration of Eq. (1) at different branching ratios. Experimental branching ratios were determined by χ^2 minimization between the experimental data (normalized to a spectrum taken with the pump beam blocked), and the theoretical spectra calculated at the experimental intensities. Error estimates for individual measurements were found by reevaluating Eq. (1) holding the branching

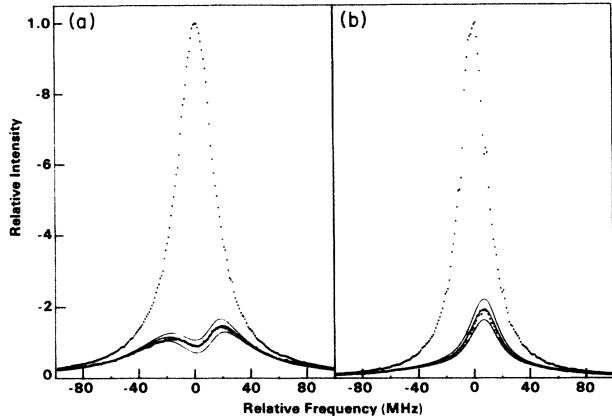


FIG. 3. Experimental spectra taken at (a) moderate pump and probe laser intensities ($I_{\text{pump}} = 26 \text{ mW/cm}^2$ and $I_{\text{probe}} = 20 \text{ mW/cm}^2$) over a 1.025-cm path length and (b) high pump intensity and low probe intensity ($I_{\text{pump}} = 162 \text{ mW/cm}^2$ and $I_{\text{probe}} = 4.4 \text{ mW/cm}^2$) over a 0.44-cm path length. The solid curves are model calculations with branching ratios of 400, 450, and 500 (bottom to top). Upper point spectra recorded with pump laser beam blocked.

ratio constant at the determined value and varying pump and probe laser intensities in the calculations. Table I shows the results obtained at a variety of pump and probe intensities and pump path lengths.

The observed asymmetry in Fig. 3(a) and the shift in 3(b) are due to recoil shift. Atoms which make it through the pump region without being trapped experience, on the average, more excitation cycles than those that are trapped, and thus the dip (due to the trapped atoms) is shifted less than the rest of the line profile. The degree of bimodal behavior depends on relative saturated bandwidths of the pump and probe lasers. When $I_{\text{pump}} \leq I_{\text{probe}}$ the lobes are most pronounced. When the effective pump bandwidth is greater than the probe [Fig. 3(b)] the low-frequency lobe is suppressed. The case where $I_{\text{pump}} \sim I_{\text{probe}} \sim I_{\text{sat}}$ [Fig. 3(a)] provided the best test of the model as line shapes (asymmetry and spacing of the two lobes, depth of inversion, etc.) were most sensitive to all experimental parameters in this region. Measurements performed using a high pump intensity and a weak probe removed, to first order, dependency on pump

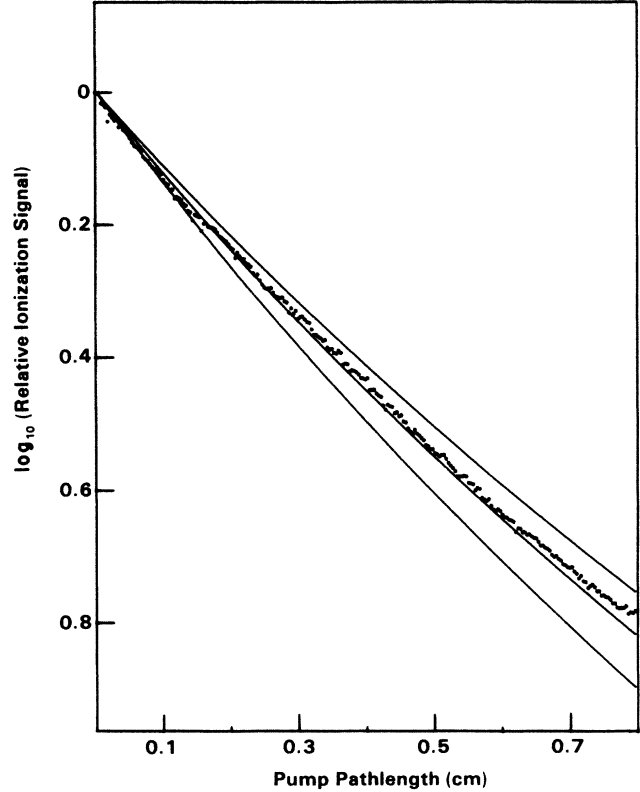


FIG. 4. Decay of the two-level population due to increased pump ($I = 26 \text{ mW/cm}^2$) path length with laser frequency fixed on line center. Points are the experimental data and solid lines the model calculation with branching ratios of 400, 450, and 500 (bottom to top.)

intensity and spatial distribution.

Figure 4 shows a typical result for decay experiments. The curvature away from simple exponential decay is due primarily to the velocity distribution, but there is also some contribution from the recoil shift which reduces the effective excitation rate with increasing pump path length. Again, χ^2 minimization between decay curves calculated using Eq. (1) and the experimental data was used to determine branching ratios. The results agree well with the frequency scan measurements. However, they are somewhat less precise with branching ratio

TABLE I. Experimental parameters and branching determinations.

Data set no.	Pump path length (cm)	Pump laser intensity (mW/cm^2)	Probe laser intensity (mW/cm^2)	Branching ratio
1	1.025	26	20	433 ± 40
2	1.025	26	20	454 ± 40
3	1.025	26	20	452 ± 40
4	0.44	162	4.4	442 ± 25
5	0.44	162	13.3	413 ± 25
6	0.44	162	4.4	453 ± 27
7	0.248	10.1	1.36	411 ± 50
Average for all measurements				437 ± 19

values ranging from 400 to 510. The precision is reduced because these measurements are sensitive to spatial variations in the pump beam intensity whereas the frequency scans are sensitive (to first order) only to the integrated pump intensity. The sharp initial drop in Fig. 4, due to an uncompensated diffraction fringe from the pump beam mask, is the most pronounced example of this intensity dependence. This also adds a degree of freedom in fitting of calculated curves to the experimental data since the starting channel for exposure is not precisely defined. Because of these limitations, branching ratios obtained from fitting the fixed frequency decay curves are used only as confirmation of the quantitative results given in Table I.

Although the standard deviation for branching ratios given in Table I is ± 19 , we allow another 5% for other possible systematic errors such as the uncertainty in the value used for the lifetime of the 1P_1 state²³ and the absolute calibration of power meters. Thus we give as a final result for the determined branching ratio a value of 440 ± 40 . While this value is greater than those recently determined to be around 300,^{11,15,16} it is less than the value of 550 recalculated¹⁴ from data of Ref. 7 and the value of 600 from theoretical calculations.¹² It is in

reasonable agreement with other theoretical values of 380 and 430 given in Ref. 14. It is difficult to assess a "best" value for the branching ratio, especially since the literature abounds with references to unpublished work, private communications, and the recalculation of others' data. However, we are confident of our measurements for a number of reasons: The structure of line inversion spectra [Fig. 3(a)] provides an excellent test of the model with high sensitivity towards all experimental parameters, uncertainties due to pump power can be reduced by saturation, results are in excellent agreement over a wide range of experimental conditions, and they are in agreement with the fixed frequency decay measurements.

ACKNOWLEDGMENTS

Discussions with T. J. Whitaker and B. D. Cannon and their review of this work are gratefully acknowledged. This work was funded by the Office of Basic Energy Sciences of the U.S. Department of Energy (DOE) and performed under DOE Contract No. DE-AC06 76RLO 1830.

¹S. Chu, L. Hollberg, J. W. Bjorkholm, A. Cable, and A. Ashkin, *Phys. Rev. Lett.* **55**, 48 (1985).

²A. Fischer and I. V. Hertel, *Z. Phys. A* **304**, 103 (1982).

³B. A. Bushaw, T. J. Whitaker, B. D. Cannon, and R. A. Warner, *J. Opt. Soc. Am. B* **2**, 1547 (1985).

⁴A. F. Bernhardt, D. E. Duerre, J. R. Simpson, and L. L. Wood, *Opt. Commun.* **16**, 169 (1976).

⁵B. D. Cannon and T. J. Whitaker, *Appl. Phys. B* **38**, 57 (1985).

⁶C. W. Bauschlicher, Jr., R. L. Jaffe, S. R. Langhoff, F. G. Mascarello, and H. Partridge, *J. Phys. B* **18**, 2147 (1985).

⁷A. F. Bernhardt, D. E. Duerre, J. R. Simpson, and L. L. Wood, *J. Opt. Soc. Am.* **66**, 416 (1976).

⁸L. O. Dickie and F. M. Kelly, *Can. J. Phys.* **49**, 2630 (1971).

⁹P. Hafner and W. H. E. Schwarz, *J. Phys. B* **11**, 2975 (1978).

¹⁰L. Jahreiss and M. C. E. Huber, *Phys. Rev. A* **31**, 692 (1985).

¹¹D. A. Lewis, J. Kumar, M. A. Finn, and G. W. Greenlees, *Phys. Rev. A* **35**, 131 (1987).

¹²P. McCavert and E. Trefftz, *J. Phys. B* **7**, 1270 (1974).

¹³E. G. Myers, C. J. Bell, P. G. Pappas, and D. E. Murnick, *Phys. Rev. A* **33**, 2798 (1986).

¹⁴S. Niggli and M. C. E. Huber, *Phys. Rev. A* **35**, 2908 (1987).

¹⁵A. Kallenback and M. Kock, *Phys. Rev. A* **35**, 437 (1987).

¹⁶S. Trajmar, J. C. Nickel, and T. Antoni, *Phys. Rev. A* **34**, 5154 (1986).

¹⁷P. A. Bokhan, *Kvant. Elektron. (Moscow)* **13**, 1595 (1986) [*Sov. J. Quantum Electron.* **16**, 1041 (1986)].

¹⁸R. J. Cook, *Phys. Rev. A* **22**, 1078 (1980).

¹⁹B. A. Bushaw, B. D. Cannon, G. K. Gerke, and T. J. Whitaker, *Opt. Lett.* **11**, 422 (1986).

²⁰C. M. Klimcak and J. C. Camparo, *Phys. Rev. A* **30**, 1791 (1984).

²¹P. Jacquinet, in *High-Resolution Laser Spectroscopy*, edited by K. Shimoda (Springer-Verlag, Berlin, 1976), pp. 51–93. Equation (2) gives the intensity distribution within the atomic beam. The number density distribution still follows the Boltzmann form of $\alpha^{-3}v^2 \exp(-v^2/\alpha^2)$. The multiplication by t (which is proportional to $1/v$) in the expansion of the probe detector function [Eq. (6)] effectively returns the intensity distribution to a density distribution.

²²R. J. Cook, *Opt. Commun.* **35**, 347 (1980).

²³F. M. Kelly and M. S. Mathur, *Can. J. Phys.* **49**, 2630 (1977).